International Journal of Fluid Mechanics & Thermal Sciences
2024; 10(1): 1-14
http://www.sciencepublishinggroup.com/j/ijfmts
doi: 10.11648/j.ijfmts.20241001.11
ISSN: 2469-8105 (Print); ISSN: 2469-8113 (Online)

Unsteady MHD Nanofluid Flow Through a Divergent Conduit with Chemical Reaction and Radiation

Valarie Nyabuti[1, *], Phineas Roy Kiogora[2], Edward Onyango[2], Eunice Nyawade[3]

[1]Department of Mathematics, Pan African University Institute of Basic Sciences, Technology and Innovation, Nairobi, Kenya
[2]Department of Pure and Applied Mathematics, Jomo Kenyatta University of Agriculture and Technology, Nairobi, Kenya
[3]Department of Chemistry, Jomo Kenyatta University of Agriculture and Technology, Nairobi, Kenya

Email address:

valarienyakerario@gmail.com (Valarie Nyabuti), prkiogora@jkuat.ac.ke (Phineas Roy Kiogora),
edward.onyango@jkuat.ac.ke (Edward Onyango), enyawade@jkuat.ac.ke (Eunice Nyawade)
*Corresponding author

To cite this article:

Valarie Nyabuti, Phineas Roy Kiogora, Edward Onyango, Eunice Nyawade. (2024). Unsteady MHD Nanofluid Flow Through a Divergent Conduit with Chemical Reaction and Radiation. *International Journal of Fluid Mechanics & Thermal Sciences, 10*(1), 1-14.
https://doi.org/10.11648/j.ijfmts.20241001.11

Received: January 23, 2024; **Accepted:** February 2, 2024; **Published:** February 28, 2024

Abstract: Inefficient heat transfer rates have resulted in high energy consumption costs in heat exchanger systems. In this study, unsteady MHD(Magneto-hydrodynamics) Nanofluid flow (Silver-water) through a divergent conduit with chemical reaction and radiation is investigated. The chemical reactions taking place within the Nanofluid are considered to be of first order with the radiation effects being in a steady state. The governing partial differential equations have been transformed into ordinary differential equations using similarity transformations. The resulting system of non-linear ordinary differential equations is then solved using the spectral collocation method and implemented in MATLAB software. The results for velocity, temperature, and concentration profiles are presented graphically and discussed. It was observed that increasing the Reynolds number and Hartmann number led to an increase in the velocity profile. Increasing the Eckert number and Joule heating parameter increased the temperature profile while increasing the radiation parameter led to a decrease in the temperature of the Nanofluid. The concentration of the Nanofluid increased with an increase in the Soret number and Chemical reaction parameter while the concentration decreased with an increase in the Schmidt number. The findings have practical applications in designing and optimizing heat exchangers by maximizing heat transfer thus contributing to the sustainability of geothermal power generation in the energy industry.

Keywords: MHD, Unsteady, Nanofluid, Divergent Conduit, Chemical Reaction, Radiation

1. Introduction

As the world population is growing, there is an increasing energy demand. The need to provide clean and renewable energy without affecting the environment is inevitable. To improve the levels of clean energy produced, alternative methods have come up such as Geothermal sources of energy.

Converging-diverging tubes(Venturi tubes)were first designed by Giovanni Battista Venturi to experiment effects of fluid pressure reduction while flowing through chokes (Venturi effect). Later on, Osborne Reynolds conducted the first experiment by investigating convergent-divergent duct flows. He used a water channel and observed the velocity profile of the flow as it passed through the convergent section into the divergent section. This work established the fundamental understanding of convergent-divergent flows and provided the basis for further research in this area.

A study on the effect of heat and mass transfer on unsteady MHD Nanofluid flow through a convergent-divergent channel was carried out by [1]. They used the collocation method and observed that the nanoparticle volume fraction decreased the velocity of the Nanofluid in the divergent section while the volume fraction increased the velocity of the Nanofluid in the convergent section. They also observed that the velocity and temperature increased with an increase in the heat generation

for both convergent and divergent channels and that the concentration of the Nanofluid decreased with an increase in heat generation parameters for both convergent and divergent channels.

Geometric and thermo-hydrodynamic effect on a 3D converging-diverging channel was researched by [2]. They analyzed the heat transfer properties of a 3D converging-diverging channel. They utilized the Taguchi and ANFIS techniques to optimize Reynolds, Hartmann numbers, Nanofluid volume fraction, and geometric parameters of the channel. They observed that the Reynolds number, Hartmann number, and Nanofluid volume fraction play more significant roles in improving the thermal and hydrodynamic performance of the channel than geometric parameters. The results showed that the increase in the Nanofluid volume fraction caused the most significant increase in the Nusselt number.

Chemical reactions in Nanofluids lead to changes in the properties of the fluid. The effects of chemical reactions have been researched and the chemical models obtained have been applied in various industries. Heat and mass transfers in a two-phase stratified turbulent fluid flow in a geothermal pipe with chemical reaction was investigated by [3]. They used the finite difference method to solve the governing equations. They established that increasing the Eckert number, Prandtl number, and angle of inclination led to an increase in the rate of heat transfer while increasing the Reynolds number, Chemical reaction parameter and angle of inclination significantly increased the mass transfer rate. They also observed that the skin friction decreased with an increase in the Reynolds number and that decreasing the chemical reaction parameter decreased the concentration of the geothermal fluid which caused corrosion of geothermal pipes.

A study on Hydro-magnetic surface-driven flow between two parallel vertical plates in the presence of chemical reaction and induced magnetic field was conducted by [4]. They applied the numerical approximation finite difference method to solve the equations numerically. They observed that an increase in the chemical reaction parameter leads to a decrease in the fluid concentration. This was caused by the negative chemical reaction which reduced the concentration boundary layer thickness and increased the mass transfer.

The Soret-Dufour effects on MHD chemically reacting fluid flow via diverging and converging channels were examined by [5]. Analytical solutions of existing flow equations were obtained by HAM (Homotopy Analysis Method) and ADM (Adomian's Decomposition Method). They revealed that when there was an increase in Reynolds number, the opposite variations were observed in temperature profiles of convergent and divergent channels.

Radiation affects the temperature and energy balance of any fluid system by influencing the flow dynamics. The effects of thermal radiation on the flow of Jeffery fluid in converging and diverging stretchable channels were investigated by [6]. They used the Adomian decomposition method to obtain solutions. They observed that an increase in the values of the Reynolds number reduced the velocity of the shrinking divergent channel and consistently increased the shrinking convergent channel velocity.

Heat and mass transfer of radiative and chemical reactive effects on MHD Nanofluid over an infinite moving vertical plate was analyzed by [7]. They used the perturbation method to solve the dimensionless boundary layer equations with various thermo-physical properties taken into account. They observed that the velocity of the Nanofluid increased as the volume fraction of solid particles increased and as the thermal radiation parameter rose. They also concluded that Cu-water Nanofluid was a better thermal conductor when compared with conventional fluids such as water.

The radiation effect on Magneto-Hydrodynamic flow with induced magnetic field and Newtonian heating/cooling using an analytic approach was examined by [8]. The MHD flow which was natural convective was electrically charged through two vertical insulated walls. They observed that radiation raised the velocity, the temperature field, the induced magnetic field, and the current density field in view of enhancing the thickness of the boundary layer.

Two-phase convergent Jeffery-Hamel flow in a geothermal pipe concentrated with silica particles and thermophoresis was studied by [9]. They used the BVP4c collocation method to solve the nonlinear ODEs. They established that the unsteadiness parameter significantly influenced the velocity, temperature, and concentration in both the gaseous and the liquid phase, secondly the Reynolds number effect in the gaseous phase velocity was more significant in comparison to the liquid phase, thirdly the variation in heat transfer as a result of the Prandtl number was more significant in comparison to the liquid phase, fourthly there was a significant effect of the control factor introduced in the concentration equation to counter silica polymerization.

A study on the effect of radiation on the flow and heat transfer over an unsteady stretching sheet was conducted by [10]. They discovered that the effect of the radiation parameter on the heat transfer rate was found to be more noticeable at larger values of the unsteadiness parameter and Prandtl number. Extensive research has been done under unsteady MHD Nanofluid flow through a convergent-divergent channel. However, previous research has given little attention to chemical reactions and radiation. This present study extends the work of [1] by incorporating both chemical reaction and radiation in unsteady MHD Nanofluid flow through a divergent conduit.

2. Mathematical Formulation

Consider two-dimensional MHD Nanofluid flow through a divergent conduit as shown in figure 1. The Nanofluid is incompressible and of non-linear viscosity of the $k-\omega$ model. The fluid flow is unsteady and described by the cylindrical polar coordinate system (r,θ,z). $|\alpha| > 0$, represents the diverging section of the flow field domain. The flow is assumed to be purely radial and satisfying the no-slip condition. This present study considered the magnetic field to be constant and uniform. The power law model has been

used to describe the non-Newtonian behavior of the fluid. The chemical reactions within the Nanofluid were considered to be of first-order and the radiation effects were in a steady state.

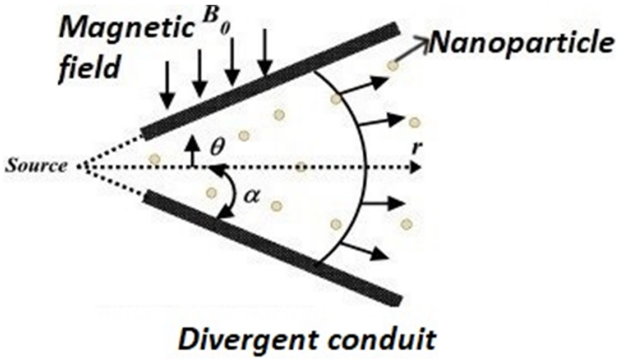

Figure 1. *Flow geometry.*

The governing equations are continuity, conservation of momentum, energy, and concentration. The velocity of the Nanofluid is given by:

$$\vec{q} = \vec{q}(r, \theta, t) \tag{1}$$

From the assumptions presented, the specific governing equations in cylindrical coordinates are expressed as follows:

Equation of Continuity

$$\frac{\rho_{nf}}{r}\frac{\partial(ru_r)}{\partial r} = 0 \tag{2}$$

Equation of Conservation of Momentum

$$\hat{r}: \rho_{nf}\frac{\partial u_r}{\partial t} = -\frac{\partial p}{\partial r} + 2\frac{\partial \mu}{\partial r}\frac{\partial u_r}{\partial r} + \frac{1}{r^2}\frac{\partial \mu}{\partial \theta}\frac{\partial u_r}{\partial \theta} + \mu\left[\frac{1}{r^2}\frac{\partial^2 u_r}{\partial \theta^2} + 2\left(\frac{\partial^2 u_r}{\partial r^2} + \frac{1}{r}\frac{\partial u_r}{\partial r} - \frac{u_r}{r^2}\right)\right] - \rho_{nf}u_r\frac{\partial u_r}{\partial r} - \sigma B_0^2 u_r\hat{r} \tag{3}$$

$$\hat{\theta}: 0 = -\frac{1}{r}\frac{\partial p}{\partial \theta} + \frac{1}{r}\frac{\partial \mu}{\partial r}\frac{\partial u_r}{\partial \theta} + 2\frac{u_r}{r^2}\frac{\partial \mu}{\partial \theta} + 2\frac{\mu}{r^2}\frac{\partial u_r}{\partial \theta} + \mu\left[\frac{1}{r}\left(\frac{\partial^2 u_r}{\partial r \partial \theta} + \frac{1}{r}\frac{\partial u_r}{\partial \theta}\right)\right] \tag{4}$$

Equation of Energy

$$\begin{aligned}\frac{\partial T}{\partial t} + u_r\frac{\partial T}{\partial r} =& \frac{k_{nf}}{\rho_{nf}C_p}\left[\frac{1}{r}\frac{\partial}{\partial r}\left(r\frac{\partial T}{\partial r}\right) + \frac{1}{r^2}\frac{\partial^2 T}{\partial \theta^2}\right] + \frac{2\mu}{\rho_{nf}C_p}\left[\left(\frac{\partial u_r}{\partial r}\right)^2 + \left(\frac{u_r}{r}\right)^2 + \right] + \\ & \frac{\mu}{\rho_{nf}C_p}\left[\left(\frac{1}{r}\frac{\partial u_r}{\partial \theta}\right)^2\right] + \frac{\sigma B_0^2 u_r^2}{\rho_{nf}C_p} - \frac{1}{\rho_{nf}C_p}\frac{\partial}{\partial r}\left(q_{r,rad}\right) - \frac{1}{r\rho_{nf}C_p}\frac{\partial}{\partial \theta}\left(q_{\theta,rad}\right)\end{aligned} \tag{5}$$

By Rosseland's approximation [11] and [12], the radiative heat flux for thermal radiation is given by:

$$q_{r,rad} = -\frac{4\sigma^*}{3k_{nf}}\frac{\partial T^4}{\partial r} \tag{6}$$

$$q_{\theta,rad} = -\frac{4\sigma^*}{3k_{nf}}\frac{\partial T^4}{\partial \theta} \tag{7}$$

where σ^* is the Stefan-Boltzmann constant and k_{nf} is the mean absorption coefficient of the Nanofluid.

Equation of Concentration

$$\frac{\partial C}{\partial t} + \frac{u_r}{r}\frac{\partial (rC)}{\partial r} = D_{nf}\left(\frac{1}{r}\frac{\partial}{\partial r}\left(r\frac{\partial C}{\partial r}\right) + \frac{1}{r^2}\frac{\partial^2 C}{\partial \theta^2}\right) - k_r(C - C_\infty) + \frac{D_{nf}K_t}{T_\infty}\left(\frac{\partial T}{\partial r}\hat{r} + \frac{1}{r}\frac{\partial T}{\partial \theta}\hat{\theta}\right) \tag{8}$$

Due to the Non-Newtonian nature of the Nanofluid, the Power Law model implemented expressed the viscosity as:

$$\mu = \mu_0 g^{n-1}(\theta) \tag{9}$$

where θ is a subset of angle α. A dilatant fluid is a type of non-Newtonian fluid that exhibits shear-thickening behavior whereby its viscosity increases with shear rate. For this study, we considered a dilatant fluid where $n > 1$. Therefore, letting:

$$g(\theta) = \theta^c, \tag{10}$$

for $c > 1$ where c is an arbitrary constant.

Then equation (9) will be expressed as:

$$\mu = \mu_0 \theta^{c(n-1)} \tag{11}$$

The boundary conditions considered are as follows:

At the center line, $\theta = 0$:

$$u_r = u_\infty, \frac{\partial u_r}{\partial \theta} = 0, T = T_\infty, \frac{\partial T}{\partial \theta} = 0, C = C_\infty, \frac{\partial C}{\partial \theta} = 0 \tag{12}$$

On the wall, $\theta = \alpha$:

$$\frac{\partial u_r}{\partial \theta} = -\gamma u(\theta), T = T_\omega, C = C_\omega \tag{13}$$

where u_∞ is the velocity at the center line, α is the wedge angle and $\gamma \geq 0$ is the friction coefficient factor.

Similarity transformation has been used to reduce the governing non-linear partial differential equations into non-linear ordinary differential equations. From [13] and [14], the similarity transformation of velocity is given as:

$$u_r(r, \theta, t) = -\frac{Q}{r}\frac{1}{\delta^{m+1}}F(\eta) \tag{14}$$

where Q is the planar volumetric flow rate, m is a constant related to the angle α, δ is the time dependent length scale, and F is the dimensionless fluid velocity. The similarity transformations for temperature and concentration are given by:

$$\frac{\omega(\eta)}{\delta^{m+1}} = \frac{T - T_\omega}{T_\infty - T_\omega} \tag{15}$$

$$\frac{\phi(\eta)}{\delta^{m+1}} = \frac{C - C_\omega}{C_\infty - C_\omega} \tag{16}$$

where $\omega(\eta)$ denotes the dimensionless temperature, $\phi(\eta)$ denotes the dimensionless concentration and η is a dimensionless parameter given as:

$$\eta = \frac{\theta}{\alpha} \tag{17}$$

Applying the transformations of equations 14, 15 and 16 into equations 2, 3, 4, 5 and 8 yielded:

$$\frac{(m+1)r^{m+1}}{\delta^{m+1}}\left(\frac{\rho_{nf}\delta^m}{\mu_0 r^{m-1}}\frac{d\delta}{dt}\right)F'(\eta) + c(n-1)c(n-2)\theta^{c(n-3)}F'(\eta) - \frac{2Q\rho_{nf}}{\mu_0}\frac{1}{\delta^{m+1}}F(\eta)F'(\eta) + c(n-1)\theta^{c(n-2)}$$
$$[2F''(\eta) + 4F(\eta)] + \theta^{c(n-1)}[F'''(\eta) + 4F'(\eta)] - \frac{\sigma B_0^2 r^2}{\mu_0}F'(\eta) = 0 \tag{18}$$

$$\left(\frac{k_{nf}}{\rho_{nf}C_p}\frac{\rho_{nf}}{\mu_0} + r\frac{16\sigma^*}{3k_{nf}\mu_0 C_p}T_\infty^3\right)\omega''(\eta) + \frac{(m+1)r^{m+1}}{\delta^{m+1}}\left(\frac{\rho_{nf}\delta^m}{\mu_0 r^{m-1}}\frac{d\delta}{dt}\right)\omega(\eta) + \frac{\theta^{c(n-1)}}{C_p}\frac{Q^2}{r^2(T_\infty - T_\omega\delta^{m+1}}$$
$$[4(F(\eta))^2 + (F'(\eta))^2] + \frac{\sigma B_0^2}{C_p\mu_0(T_\infty - T_\omega)\delta^{m+1}}Q^2(F(\eta))^2 = 0 \tag{19}$$

$$D_{nf}\frac{\rho_{nf}}{\mu_0}\phi''(\eta) + \frac{(m+1)r^{m+1}}{\delta^{m+1}}\left(\frac{\rho_{nf}\delta^m}{\mu_0 r^{m-1}}\frac{d\delta}{dt}\right)\phi(\eta) - \frac{k_r\rho_{nf}r^2}{\mu_0}[\phi(\eta) - \delta^{m+1}] + \frac{D_{nf}K_t}{T_\infty}\frac{\rho_{nf}r}{\mu_0}\frac{(T_\infty - T_\omega)}{(C_\infty - C_\omega)}\omega'(\eta) = 0 \tag{20}$$

The following dimensionless parameters are observed from equations 18-20:

Reynolds number: $Re = \frac{Q\rho_{nf}}{\mu_0}$, Hartmann number: $Ha = B_0 r\sqrt{\frac{\sigma}{\mu_0}}$, Unsteadiness Parameter: $\lambda = \frac{\rho_{nf}\delta^m}{\mu_0 r^{m-1}}\frac{d\delta}{dt}$, Prandtl number: $Pr = \frac{\mu_0}{\rho_{nf}\alpha}$ where $\alpha = \frac{k_{nf}}{\rho_{nf}C_p}$, Radiation parameter: $Rd = \frac{16\sigma^*}{3k_{nf}\mu_0 C_p}T_\infty^3$, Eckert number: $Ec = \frac{Q^2/r^2}{C_p(T_\infty - T_\omega)}$, Joule heating parameter: $J = \frac{\sigma B_0^2 Q^2}{C_p\mu_0(T_\infty - T_\omega)}$, Schmidt number: $Sc = \frac{\upsilon}{D_{nf}}$ where $\upsilon = \frac{\mu_0}{\rho_{nf}}$, Soret number: $Sr = \frac{D_{nf}K_t}{\upsilon T_\infty}\frac{(T_\infty - T_\omega)}{(C_\infty - C_\omega)}$, Chemical reaction parameter: $\Gamma = \frac{k_r\rho_{nf}r^2}{\mu_0}$

Substituting the non-dimensional parameters into equations 18, 19 and 20 yielded:

$$\frac{(m+1)r^{m+1}}{\delta^{m+1}}\lambda F'(\eta) + c(n-1)c(n-2)\theta^{c(n-3)}F'(\eta) - 2Re\frac{1}{\delta^{m+1}}F(\eta)F'(\eta) + c(n-1)\theta^{c(n-2)}[2F''(\eta) + 4F(\eta)] + \theta^{c(n-1)}[F'''(\eta) + 4F'(\eta)] - Ha^2F'(\eta) = 0 \tag{21}$$

$$\left(\frac{1}{Pr} + rRd\right)\omega''(\eta) + \frac{(m+1)r^{m+1}}{\delta^{m+1}}\lambda\omega(\eta) + \frac{Ec}{\delta^{m+1}}\theta^{c(n-1)}[4(F(\eta))^2 + (F'(\eta))^2] + \frac{J}{\delta^{m+1}}(F(\eta))^2 = 0 \tag{22}$$

$$\frac{1}{Sc}\phi''(\eta) + \frac{(m+1)r^{m+1}}{\delta^{m+1}}\lambda\phi(\eta) - \Gamma[\phi(\theta) - \delta^{m+1}] + rS_r\omega'(\eta) = 0 \tag{23}$$

Transforming the boundary conditions with the transformations 14, 15 and 16:

At the center line, $\eta = 0$

$$F(0) = 1, F'(0) = 0, \omega(0) = \delta^{m+1}, \phi(0) = \delta^{m+1} \tag{24}$$

At the walls, $\eta = \alpha$

$$F'(\alpha) = -\gamma F(\alpha), \omega(\alpha) = 0, \phi(\alpha) = 0 \tag{25}$$

The Skin friction, Nusselt number, and Sherwood number are defined as:

$$C_f = \frac{-2}{\sqrt{Re\,(2-\epsilon)}}F'(0) \tag{26}$$

$$Nu = -\sqrt{\frac{Re}{(2-\epsilon)}}\,\omega'(0) \tag{27}$$

$$Sh = -\sqrt{\frac{Re}{(2-\epsilon)}}\,\phi'(0) \tag{28}$$

3. Numerical Solution

The equations (21), (22), and (23) are nonlinear Ordinary Differential Equations (ODEs) that are solved numerically. The nonlinear ODEs obtained from the current model are subject to boundary conditions and therefore numerical techniques for boundary value problems (BVPs) are employed in solving them. The Spectral Collocation method has been used in this study for solving the two-point boundary value problems (BVPs). This numerical technique approximates solutions to differential equations, particularly partial differential equations (PDEs), within a given domain. The collocation method has been demonstrated in [15] to be convergent, consistent, and stable, which are three crucial characteristics to take into account when determining the most effective approach for resolving model problems.

The model equations which are of higher-order non-linear ODEs are first reduced to first-order non-linear ODEs for convenience when solving. The following conventions were used for this study:

$$y_1 = F, y_2 = F', y_3 = F'', y_4 = \omega, y_5 = \omega', y_6 = \phi, y_7 = \phi' \tag{29}$$

The system of first-order equations is given by the matrix:

$$\begin{bmatrix} y_1' \\ y_2' \\ y_3' \\ y_4' \\ y_5' \\ y_6' \\ y_7' \end{bmatrix} = \begin{bmatrix} y_2 \\ y_3 \\ \frac{-(m+1)r^{m+1}}{\delta^{m+1}\theta^{c(n-1)}}\lambda y_2 - \frac{c(n-1)c(n-2)\theta^{c(n-3)}}{\theta^{c(n-1)}}y_2 + \frac{2Re}{\delta^{m+1}\theta^{c(n-1)}}y_1y_2 - \frac{c(n-1)\theta^{c(n-2)}}{\theta^{c(n-1)}}(2y_3 + 4y_1) + \frac{Ha^2}{\theta^{c(n-1)}}y_2 - 4y_2 \\ y_5 \\ \frac{1}{1+rRdPr}\left\{\frac{-Pr(m+1)r^{m+1}}{\delta^{m+1}}\lambda y_4 - \frac{PrEc}{\delta^{m+1}}\theta^{c(n-1)}\left(4y_1^2 + y_2^2\right) - \frac{PrJ}{\delta^{m+1}}y_1^2\right\} \\ y_7 \\ Sc\left\{\frac{-(m+1)r^{m+1}}{\delta^{m+1}}\lambda y_5 + \Gamma\left(y_6 - \delta^{m+1}\right) - rSry_5\right\} \end{bmatrix}$$

The boundary conditions 24 and 25 are also reduced to first order:

At the center line, $\eta = 0$

$$y_1(0) = 1, y_2(0) = 0, y_4(0) = \delta^{m+1}, y_6(0) = \delta^{m+1} \tag{30}$$

At the walls, $\eta = \alpha$

$$y_2(\alpha) = -\gamma y_1(\alpha), y_4(\alpha) = 0, y_6(\alpha) = 0 \tag{31}$$

4. Results and Discussion

This study presents a model that contains velocity, temperature, and concentration profiles which have been simulated to produce the following graphical results.

From figure 2, an increase in the Reynolds number resulted in to increase in the velocity of the Nanofluid. Reynolds number is the ratio of inertial forces to viscous forces. Increasing the Reynolds number significantly implies that the viscous forces are decreasing which in turn increases the velocity of the Nanofluid since motion is less opposed. Conversely, decreasing the Reynolds number implies that the viscous forces dominate leading to the motion of the Nanofluid experiencing more resistance thus decreasing the velocity of the Nanofluid.

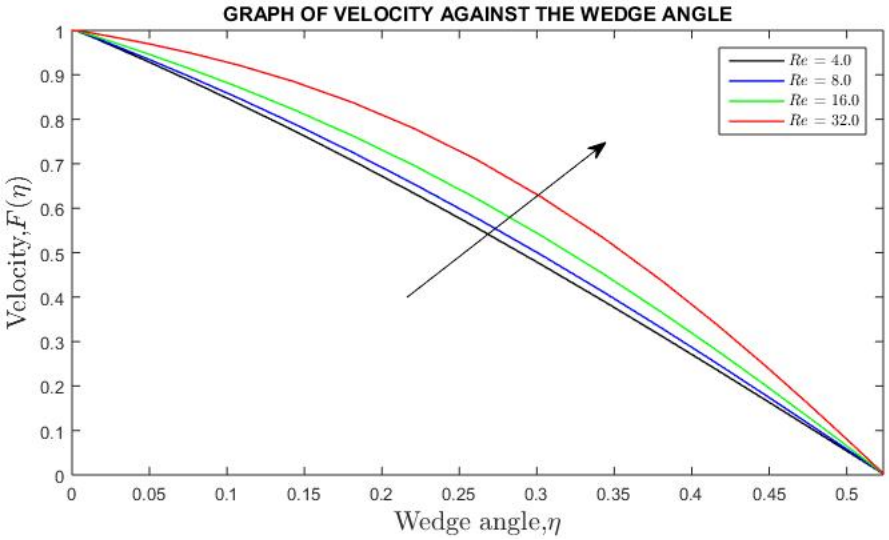

Figure 2. *Effect of varying Reynolds number on velocity profile.*

From figure 3, an increase in the Hartmann number led to a decrease in the velocity profiles. Interaction between the electrically conducting fluid and the magnetic field gives rise to the Lorentz force. This force acts in a direction perpendicular to both the magnetic field and the fluid velocity and opposes any motion of the fluid that is perpendicular to the magnetic field. Increasing the Hartmann number implies a stronger magnetic field which increases the Lorentz force acting on the Nanofluid which in turn suppresses fluid motion. Thus increasing the Hartmann numbers enhances a stabilizing effect on the Nanofluid by reducing the fluid velocity.

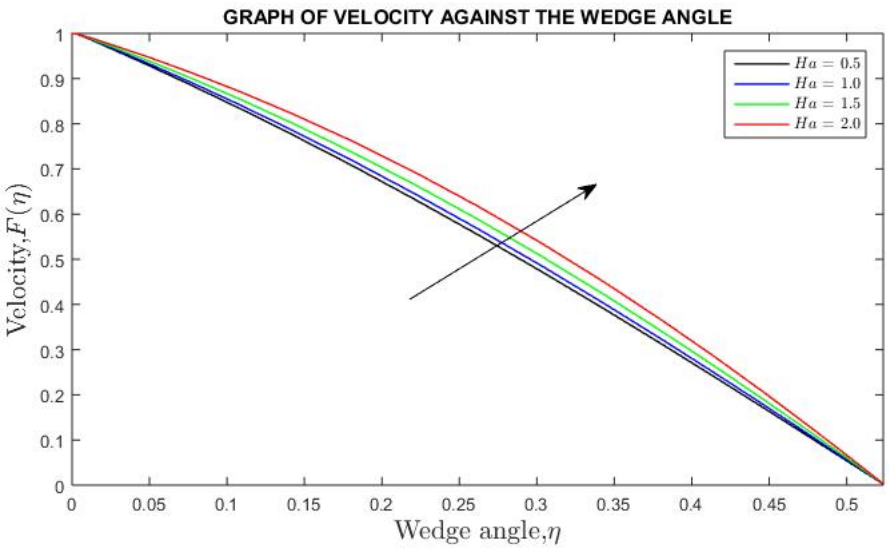

Figure 3. *Effect of varying Hartmann number on velocity profile.*

From figure 4, increasing the unsteadiness parameter led to a decrease in the velocity of the Nanofluid. Increasing the unsteadiness parameter means that the velocity is changing rapidly with time. This variability results from factors such as unsteady boundary conditions, oscillatory inflow, or time-dependent heat sources. In a rapidly changing flow, the fluid particles need to adjust to the changing conditions. This inertia in the fluid's response to changing conditions can manifest as a reduction in the mean velocity of the Nanofluid. The fluid particles cannot accelerate or maintain high velocities because they are continuously adjusting to the rapidly changing flow hence resulting in the overall reduced velocity.

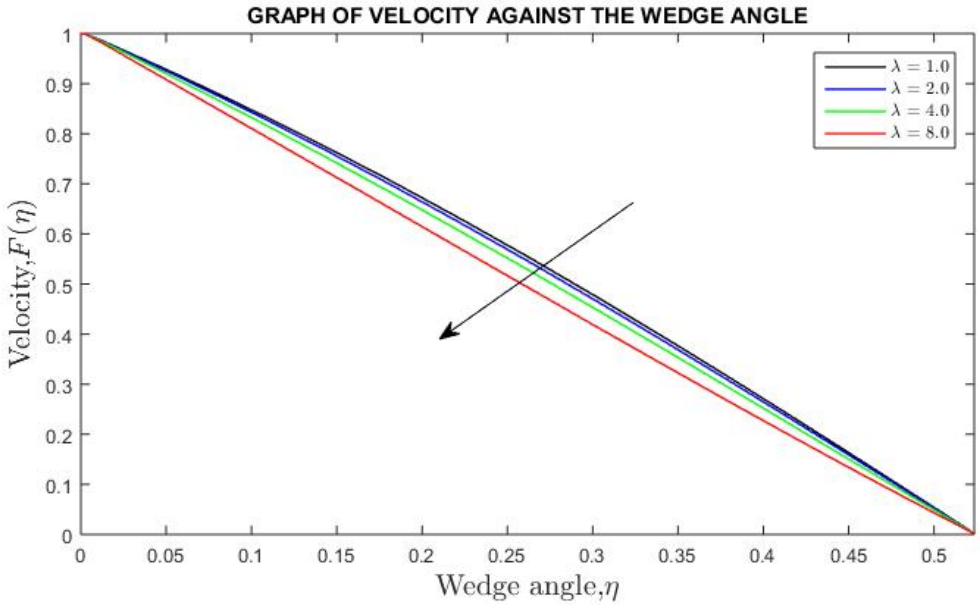

Figure 4. *Effect of varying unsteadiness parameter on velocity profile.*

From figure 5, increasing the Prandtl number relatively decreases the temperature of the Nanofluid. The Prandtl number characterizes the relative importance of momentum diffusivity (kinematic viscosity) to thermal diffusivity in the Nanofluid. Increasing the Prandtl number implies increased viscous forces and decreased thermal diffusivity. The rate of heat transfer within the Nanofluid decreases thus it takes longer for temperature changes to occur, ultimately leading to lower Nanofluid temperatures.

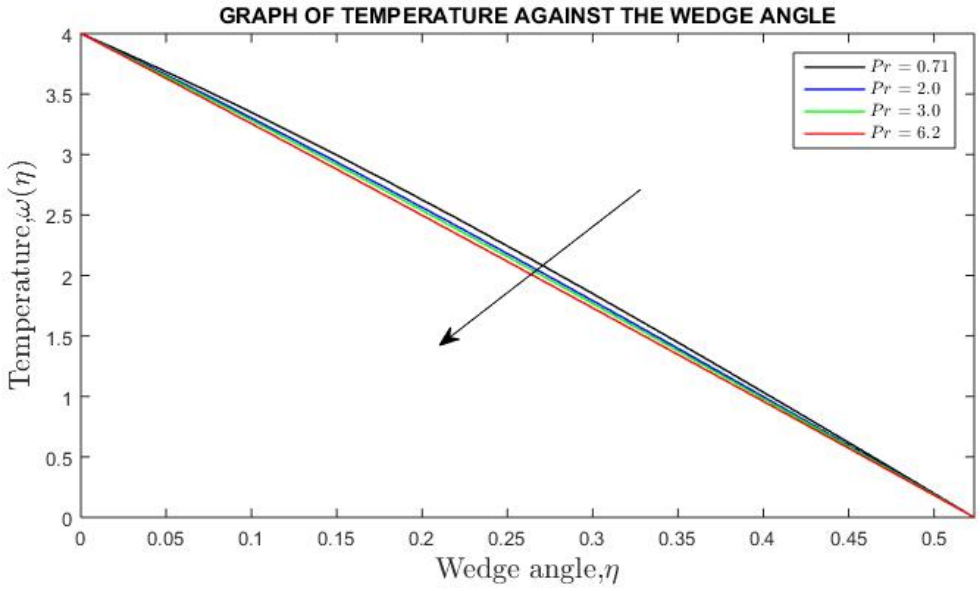

Figure 5. *Effect of varying Prandtl number on temperature profile.*

From figure 6, an increase in the Eckert number leads to an increase in the temperature of the Nanofluid. The Eckert number characterizes the relative importance of kinetic energy to internal(thermal) energy in the Nanofluid flow. Increasing this parameter indicates that the Nanofluid has a higher kinetic energy compared to its internal energy. This means that the flow is more dynamic and the effects of turbulence and viscosity lead to the conversion of kinetic energy into thermal energy which results in temperature rise within the Nanofluid.

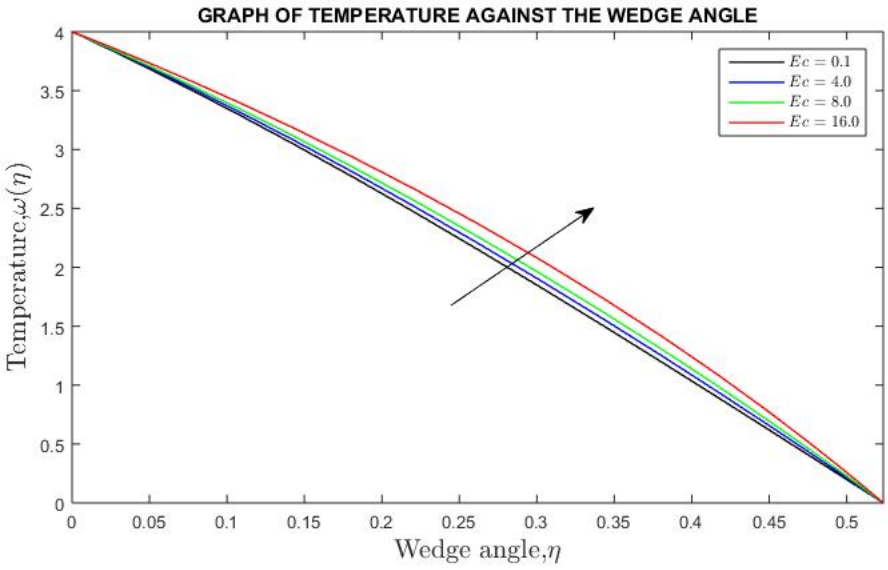

Figure 6. *Effect of varying Eckert number on temperature profile.*

From figure 7, increasing the radiation parameter typically leads to a decrease in the temperature of the Nanofluid. Increasing the radiation parameter indicates that the radiative heat transfer becomes more influential in the overall heat exchange process. However, the Nanofluid is less efficient at absorbing radiative heat. Instead, it tends to emit more heat through radiation, meaning that a greater portion of the energy in the fluid is radiated out, resulting in a cooling effect. Radiative cooling involves the emission of thermal radiation from a warmer surface to a cooler environment through radiation. Therefore, as the parameter rises, more heat is radiated away from the Nanofluid, leading to a net loss of thermal energy and thus a decrease in temperature.

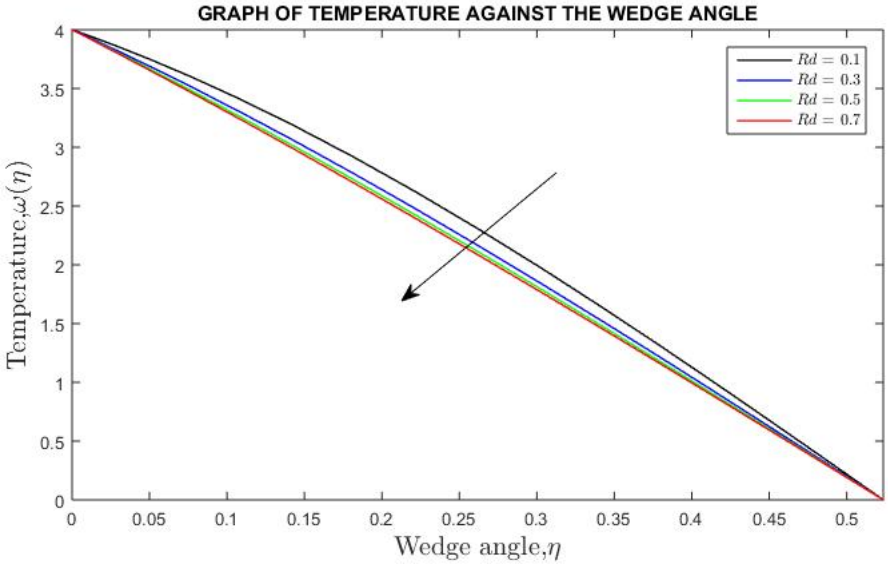

Figure 7. *Effect of varying Radiation parameter on temperature profile.*

From figure 8, increasing the Joule heating parameter leads to an increase in the temperature of the Nanofluid. The Joule heating parameter is related to the electrical resistance of the conducting medium. When the parameter increases, it indicates that the Nanofluid has higher resistance to the flow of the electrical current which results in electrical energy being converted into thermal energy. Heat is generated due to the friction of charged particles moving through the Nanofluid. This heat adds to the fluid's internal energy, leading to a temperature increase.

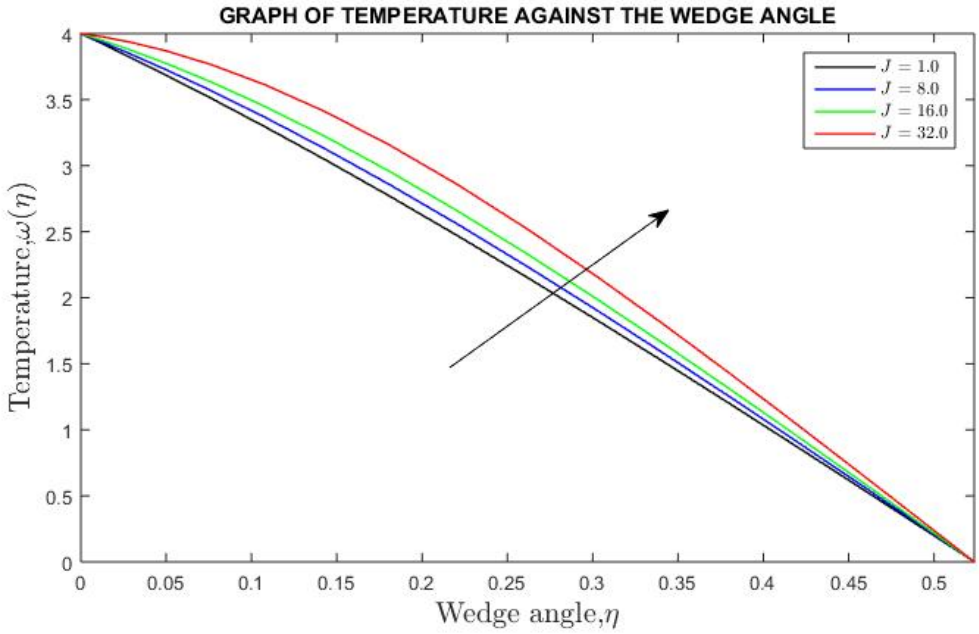

Figure 8. *Effect of varying Joule heating parameter on temperature profile.*

From figure 9, increasing the unsteadiness parameter increases the temperature of the Nanofluid. The unsteadiness parameter reflects the degree of temporal variation or unsteadiness in the flow field. Unsteady flows include time-dependent heat sources that have variations in heat input which directly impact the temperature of the Nanofluid. The variations result in increased fluid dissipation, especially in the form of viscous dissipation. This process generates heat, leading to a temperature rise in the Nanofluid.

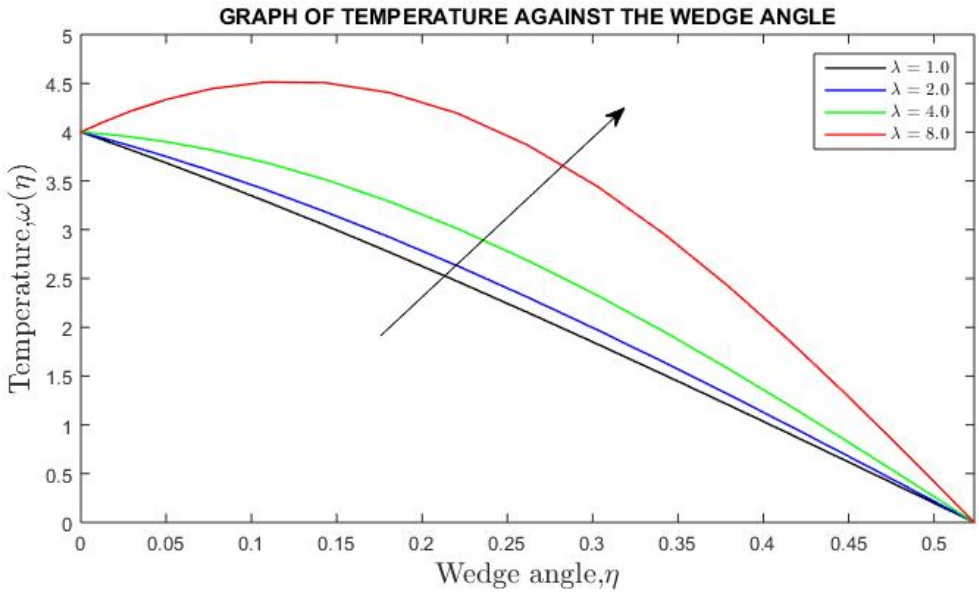

Figure 9. *Effect of varying Unsteadiness parameter on temperature profile.*

From figure 10, increasing the Schmidt number leads to a decrease in the concentration of the Nanofluid. The Schmidt number characterizes the relative importance of momentum diffusivity(kinematic viscosity) to mass diffusivity. A higher Schmidt number means that mass transfer is less efficient since mass diffusion is slowed down compared to the rate of momentum diffusion. As a result, the concentration of the Nanofluid decreases because the fluid has a harder time transporting and mixing the Nanofluid components.

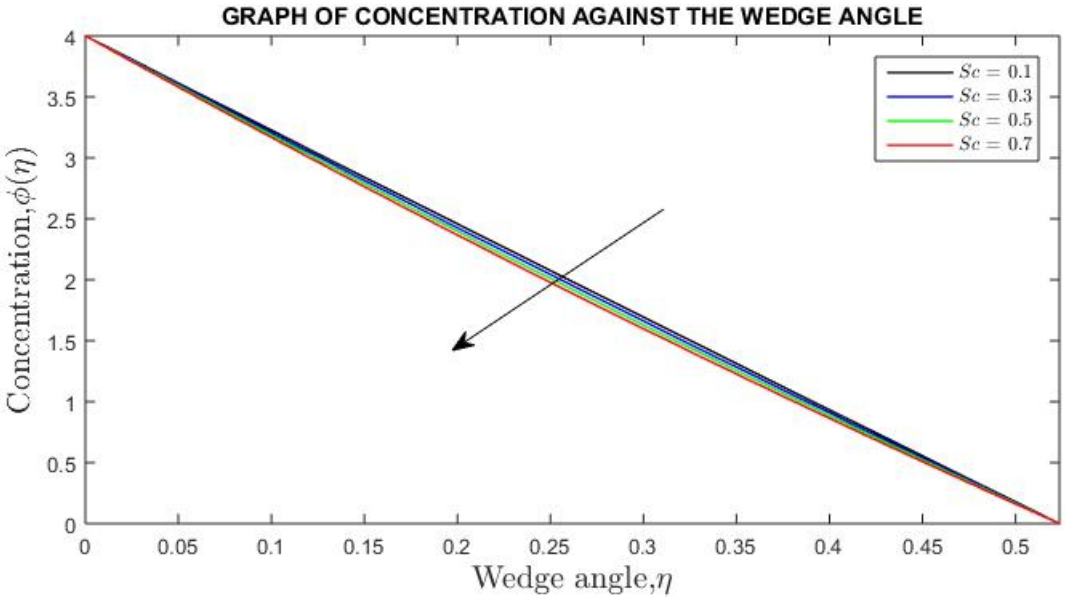

Figure 10. *Effect of varying Schmidt number on concentration profile.*

From figure 11, increasing the Soret number typically increases the concentration of the Nanofluid. Soret number characterizes the relative importance of thermal diffusion to mass diffusion. Increasing the Soret number implies that thermal diffusion is more significant compared to mass diffusion. The effect of temperature gradients on mass transfer becomes stronger hence nanoparticles migrate from regions of higher temperature to regions of lower temperature. This results in higher local concentrations of nanoparticles in the Nanofluid.

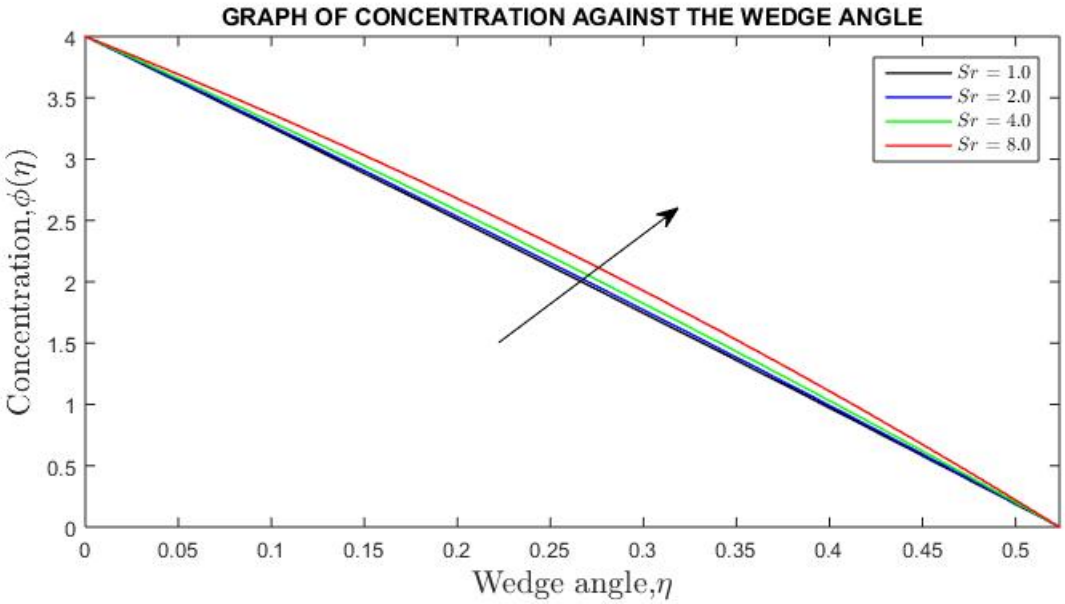

Figure 11. *Effect of varying Soret number on concentration profile.*

From figure 12, the concentration of the Nanofluid increases with an increase in the chemical reaction parameter. A higher chemical reaction parameter signifies that chemical reactions occur more rapidly within the Nanofluid. Faster chemical reactions lead to increased production of solute species or nanoparticles by generating additional components such as reaction products or by-products. This results in an increase in the concentration of the nanoparticles within the Nanofluid.

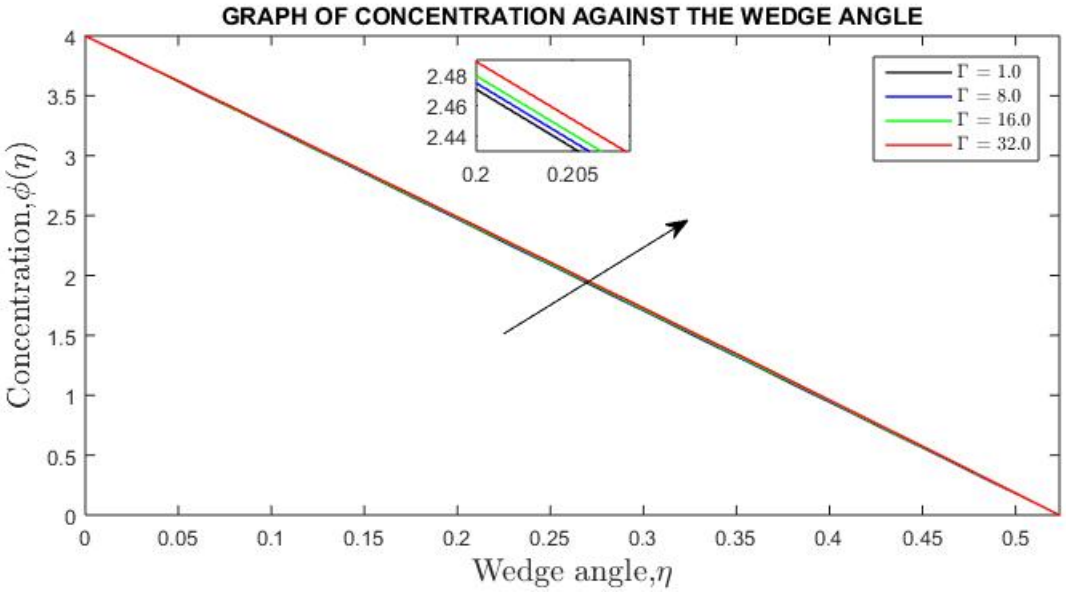

Figure 12. *Effect of varying chemical reaction parameter on concentration profile.*

From figure 13, increasing the unsteadiness parameter generally leads to an increase in the concentration of the Nanofluid. Increasing the unsteadiness parameter indicates that the flow is more dynamic and unsteady. A higher unsteadiness parameter also implies an increase in temperature over short time intervals. This leads to enhanced mixing of nanoparticles over a larger volume of the Nanofluid, resulting in higher overall concentrations because the nanoparticles are distributed more evenly.

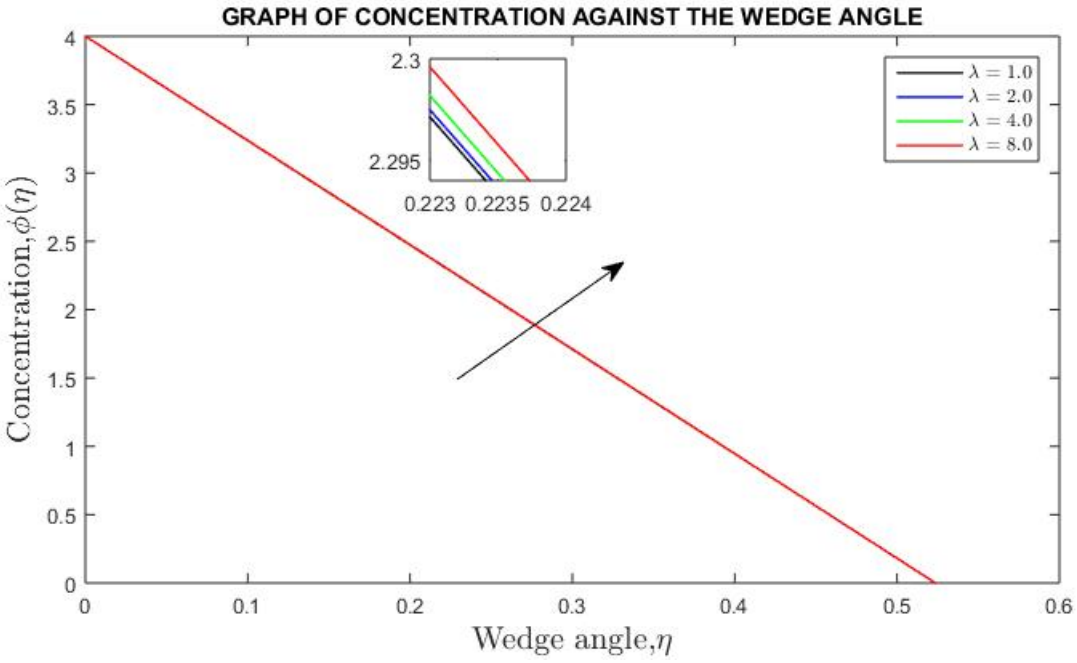

Figure 13. *Effect of varying Unsteadiness parameter on concentration profile.*

4.1. Effects of Flow Parameters on Skin Friction Coefficient

Table 1 displays the effects of Reynolds number, Hartmann number, and unsteadiness parameter on the skin friction coefficient. It is noted that as the Reynolds number increases, the skin friction coefficient reduces. Increasing the Reynolds number implies that the viscous forces are reducing which then makes the fluid experience less resistance thus reducing skin friction. Increasing the Hartmann number augments the skin friction coefficient. Increasing the Hartmann number signifies a stronger magnetic field which exerts stronger control over the fluid motion. The fluid flow is therefore restricted resulting in higher viscous forces which consequently leads to an increase in the skin friction coefficient.

Table 1. *Results of Skin friction coefficient for different physical parameters.*

Re	Ha	λ	Cf
4.00	0.50	1.00	2.19367
8.00			1.66222
16.00			1.33242
32.00			1.16428
4.00	0.50	1.00	2.19367
	1.00		2.29647
	1.50		2.47210
	2.00		2.72624
4.00	0.50	1.00	2.19367
		2.00	2.12628
		4.00	1.99436
		8.00	1.74271

4.2. Effects of Flow Parameters on Heat Transfer Rate

Table 2. *Results of heat transfer rate for different physical parameters.*

Ec	J	λ	Rd	Nu
0.10	1.00	1.00	0.10	16.84203
4.00				18.18833
8.00				19.56915
16.00				22.33079
0.10	1.00	1.00	0.10	16.84203
	8.00			17.58512
	16.00			18.43437
	32.00			20.13286
0.10	1.00	1.00	0.10	16.84203
		2.00		18.46412
		4.00		22.45800
		8.00		35.45070
0.10	1.00	1.00	0.10	16.84203
			0.30	16.14026
			0.50	15.87334
			0.70	15.73271

Table 2 displays the effects of Eckert number, Joule heating, unsteadiness parameter, and Radiation parameter on Nusselt number. The Nusselt number increases with an increase in Eckert number, Joule heating parameter, and unsteadiness parameter while it reduces with an augment in the radiation parameter. Increasing the Eckert number, Joule heating parameter and unsteadiness parameter increases the temperature of the Nanofluid which in turn enhances the heat transfer rate. Increasing the radiation parameter reduces the overall temperature of the Nanofluid through the cooling effect which results in a decrease in the Nusselt number. There is no change in the Nusselt number when the Schmidt number, Soret number, and Chemical reaction parameters are varied.

4.3. Effects of Flow Parameters on Mass Transfer Rate

Table 3 displays the effects of Schmidt number, Soret number, unsteadiness parameter, and chemical reaction parameter on the Sherwood number. Increasing these non-dimensional parameters augments the diffusion of nanoparticles. This enhances the mass transfer rate in the Nanofluid thus increasing the Sherwood number. There is very little effect of the Hartmann number and Prandtl number on the Sherwood number.

Table 3. *Results of mass transfer rate for different physical parameters.*

Sc	Sr	λ	Γ	Sh
0.10	1.00	1.00	1.00	15.87301
0.30				17.05739
0.50				18.23664
0.70				19.41080
0.10	1.00	1.00	1.00	15.87301
	2.00			16.29279
	4.00			17.13235
	8.00			18.81147
0.10	1.00	1.00	1.00	15.87301
		2.00		15.92925
		4.00		16.05042
		8.00		16.34905
0.10	1.00	1.00	1.00	15.87301
			8.00	16.82835
			16.00	17.89170
			32.00	19.93404

5. Conclusion

This study has investigated the unsteady MHD Nanofluid flow through a divergent conduit with chemical reaction and radiation. The governing equations are continuity, conservation of momentum, energy, and concentration. The effects of non-dimensional parameters on the flow variables, skin friction coefficient, Nusselt number, and Sherwood number were examined. Based on the results obtained, the following conclusions are drawn:

1. The velocity profiles increased with an increase in the Reynolds number and Hartmann number while

increasing the unsteadiness parameter significantly led to a decrease in the velocity profile.
2. The temperature profiles increased with an increase in the Eckert number, Joule heating parameter, and unsteadiness parameter while increasing the Prandtl number and radiation parameter led to a decrease in the temperature profiles.
3. The concentration profiles increased with an increase in the Soret number, chemical reaction parameter, and unsteadiness parameter while increasing the Schmidt number led to a decrease in the concentration profile.
4. The skin friction coefficient decreased with an increase in the Reynolds number and unsteadiness parameter while augmenting the Hartmann number led to an increase in the skin friction coefficient.
5. The heat transfer rate augmented with an increase in the Eckert number, Joule heating parameter, and unsteadiness parameter while increasing the radiation parameter led to a decrease in the heat transfer rate.
6. The mass transfer rate augmented with an increase in the Schmidt number, Soret number, unsteadiness parameter, and Chemical reaction parameter.

6. Recommendations

Further research can be carried out on:
1. Influence of variable magnetic field on unsteady MHD Nanofluid flow through a convergent-divergent conduit with chemical reaction and radiation.
2. Effects of chemical reaction and radiation on unsteady MHD Nanofluid of compressible flow through a convergent-divergent conduit.
3. Three-dimensional MHD Nanofluid flow through a convergent-divergent conduit with chemical reaction and radiation for turbulent flows.

Abbreviations

PDE	Partial differential equations
ODE	Ordinary differential equations
MHD	Magneto-hydrodynamics
MATLAB	Matrix Laboratory
bvp4c	boundary value problems 4^{th} order collocation
BC	Boundary Condition
HAM	Homotopy Analysis Method
ADM	Adomian Decomposition Method
ANFIS	Adaptive Neuro Fuzzy Inference System

Nomenclature

Symbol	Meaning	SI Units
C_p	Specific heat capacity	$JKg^{-1}K^{-1}$
u, v, w	velocity components	ms^{-1}
t	Time	s
P	Pressure	N/m^2
T	Temperature of the fluid	K
C	Concentration of the fluid	kg/m^3
K	Thermal conductivity	$W/(mK)$
F	Body Forces	N
D_{nf}	Mass diffusivity of nanoparticles	m^2/s
B_0	Strength of Magnetic Field	
q_{rad}	Radiative heat flux	
Re	Reynolds number	
Pr	Prandtl	
Ha	Hartmann number	
Sc	Schmidt number	
Rd	Radiation parameter	
C_f	Skin friction coefficient	
Nu	Nusselt number	
Sh	Sherwood number	
r, θ, z	Cylindrical coordinate system	
$\vec{\nabla}$	Gradient Operator	$\left(\frac{\hat{r}}{r}\frac{\partial}{\partial r}(r) + \frac{\hat{\theta}}{r}\frac{\partial}{\partial \theta} + \hat{z}\frac{\partial}{\partial z}\right)$

ORCID

0009-0007-2470-9347 (Valarie Nyakerario Nyabuti)

Acknowledgments

The authors are grateful to the Pan African University Institute for Basic Sciences, Technology, and Innovation (PAUSTI) for supporting this research. Appreciation goes to the African Union for funding this study. Gratitude also goes to Jomo Kenyatta University of Agriculture and Technology (JKUAT) for aiding this study.

Data Availability

The data used to support the findings of this study are available from the corresponding author upon request.

Conflict of Interest

The authors declare no conflict of interest.

References

[1] F. Habiyaremye, M. Wainaina, and M. Kimathi, "The effect of heat and mass transfer on unsteady mhd nanofluid flow through convergent-divergent channel," International Journal of Fluid Mechanics & Thermal Sciences, vol. 8, no. 1, pp. 10-22, 2022.

[2] M. Goharimanesh, E. A. Jannatabadi, M. Dehghani, and S. M. Javadpour, "Geometric and thermo hydrodynamic investigation of a 3d converging-diverging channel by taguchi and anfis methods," International Communications in Heat and Mass Transfer, vol. 138, p. 106285, 2022.

[3] E. M. Nyariki, M. N. Kinyanjui, and J. O. Abonyo, "Heat and mass transfers in a two-phase stratified turbulent fluid flow in a geothermal pipe with chemical reaction," Journal of Applied Mathematics and Physics, vol. 11, no. 2, pp. 484-513, 2023.

[4] M. Kinyanjui and E. R. Onyango, "Hydromagnetic surface driven flow between two parallel vertical plates in the presence of chemical reaction and induced magnetic field," Global Journal of Pure and Applied Mathematics, vol. 18, no. 1, pp. 583-612, 2022.

[5] U. Khan, N. Ahmed, and S. T. Mohyud-Din, "Thermo-diffusion, diffusion-thermo and chemical reaction effects on mhd flow of viscous fluid in divergent and convergent channels," Chemical Engineering Science, vol. 141, pp. 17-27, 2016.

[6] N. Ahmed, A. Abbasi, U. Khan, and S. T. Mohyud-Din, "Thermal radiation effects on flow of jeffery fluid in converging and diverging stretchable channels," Neural Computing and Applications, vol. 30, pp. 2371-2379, 2018.

[7] S. Arulmozhi, K. Sukkiramathi, S. S. Santra, R. Edwan, U. Fernandez-Gamiz, and S. Noeiaghdam, "Heat and mass transfer analysis of radiative and chemical reactive effects on mhd nanofluid over an infinite moving vertical plate," Results in Engineering, vol. 14, p. 100394, 2022.

[8] D. Kumar, "Radiation effect on magnetohydrodynamic flow with induced magnetic field and newtonian heating/cooling: an analytic approach," Propulsion and Power Research, vol. 10, no. 3, pp. 303-313, 2021.

[9] V. Ojiambo, M. Kinyanjui, and M. Kimathi, "A study of two-phase jeffery hamel flow in a geothermal pipe," 2018.

[10] M. Abd El-Aziz, "Radiation effect on the flow and heat transfer over an unsteady stretching sheet," International Communications in Heat and Mass Transfer, vol. 36, no. 5, pp. 521-524, 2009.

[11] A. Pantokratoras, "Natural convection along a vertical isothermal plate with linear and non-linear rosseland thermal radiation," International journal of thermal sciences, vol. 84, pp. 151-157, 2014.

[12] A. Dogonchi and D. Ganji, "Investigation of mhd nanofluid flow and heat transfer in a stretching/shrinking convergent/divergent channel considering thermal radiation," Journal of Molecular Liquids, vol. 220, pp. 592-603, 2016.

[13] J. Nagler, "Jeffery-hamel flow of non-newtonian fluid with nonlinear viscosity and wall friction," Applied Mathematics and Mechanics, vol. 38, pp. 815-830, 2017.

[14] M. A. Sattar, "Derivation of the similarity equation of the 2-d unsteady boundary layer equations and the corresponding similarity conditions," American Journal of Fluid Dynamics, vol. 3, no. 5, p. 135, 2013.

[15] J. Kierzenka and L. F. Shampine, "A bvp solver that controls residual and error," Journal of Numerical Analysis, Industrial and Applied Mathematics, vol. 3, no. 1-2, pp. 27-41, 2008.